Commensurate-incommensurate transition and strain relief patterns in monolayer C_{60} on Cd(0001)

Zilong Wang ●, Kai Sun,[*] Minlong Tao, Daxiao Yang ●, Mingxia Shi, Zuo Li ●, and Junzhong Wang[*]

School of Physical Science and Technology, Southwest University, Chongqing 400715, China

We have studied the commensurate-incommensurate phase transition, rotation epitaxy, and strain relief patterns in C_{60} overlayers grown on Cd(0001) with a low-temperature scanning tunneling microscopy. When deposited at low temperature ($\sim$200 K), C_{60} molecules form the 10×10 high-order commensurate (HOC) phase with two different half-unit cells, resembling the Si(111)-7×7 surface. Postannealing at room temperature (RT) results in the transition from HOC phase to incommensurate phase, in which strain relaxation takes place in the form of periodic vacancies and C_{60} heptamer arrays. In the case of RT deposition, parallel stripe domain walls appeared in the commensurate $2\sqrt{3}\times2\sqrt{3}$ R30° phase. These results provide essential information for understanding the strain relaxation mechanism, and the role of substrate temperatures in the process of C_{60} thin films growth.

I. INTRODUCTION

In the past decades, there have been extensive studies on the commensurate-incommensurate (C-I) phase transition in physisorbed systems and epitaxial graphene [1–6]. According to the Novaco-McTague theory, C-I phase transition occurs via the formation of domain walls (discommesuration) when adsorbate-adsorbate interaction is comparable to adsorbate-substrate interaction [7,8]. Strain is usually built in the domains and is released in domain walls. If the adsorbates are compressed in the domains, they will be stretched in domain walls and vice versa. Depending on the wall crossing energy, the domain walls may either form parallel stripe patterns or hexagonal array [1]. When the overlayer is far from commensuration, the interplay of longitudinal and transversal strains may lead to the overlayer rotation relative to the symmetry axes of substrate, i.e., orientational (rotational) epitaxy [7].

C_{60} monolayer on solid surfaces represents a model system because of the structural symmetry and rich electronic properties. A wide range of monolayer structures of C_{60} have been found on metallic or semiconducting substrates such as Au [9–12], Ag [13–16], Cu [17–19], graphite or graphene [20–23], pristine or modified Si [24–27]. Interestingly, both C-I phase transition and rotational epitaxy have been observed in the C_{60} monolayers. For example, the solitonlike domain walls induced by stress relaxation were observed in the C_{60} monolayer grown on Ge(100) [28]. Orientational epitaxy takes place in the C_{60} monolayer on Pb(111) through a lattice rotation of 20°, corresponding to a higher-order commensurate (HOC) phase [29]. For C_{60} on Cu(111), lower temperature deposition results in two metastable phases, i.e., linear-wall mazes and disordered maze patterns, which are rotated for an angle of 30° and $6 \sim 8°$ with respect to the Cu(111)

lattices [19]. In particular, the disordered-maze phase is highly compressed with a nearest-neighbor distance of 9.6 Å, representing a limiting case where the adsorbate-adsorbate interaction is dominating, while the linear-wall-maze pattern is an intermediate case where neither adsorbate-adsorbate nor adsorbate-substrate interaction is dominating.

Compared to the noble metal substrates such as Au, Ag, and Cu, the divalent hexagonal close-packed metal Cd is usually used as electrode material due to the smaller electronegativity [30–32]. Thus the interface structure of C_{60} monolayer on Cd(0001) plays a fundamental role in the electronic devices because the C_{60} molecules are contacted with metallic electrode. In this paper, C-I phase transition and strain relief patterns have been found in the C_{60} monolayer grown on Cd(0001). With substrate temperature increasing, the C_{60} monolayer shows a structure evolution from the 10×10 HOC phase to an incommensurate phase that consists of periodic vacancies and heptamer arrays, and to the $2\sqrt{3}\times2\sqrt{3}$ R30° commensurate phase with stripe domain walls. In particular, the 10×10 HOC phase has two different half-unit cells (HUCs), very similar to the Si(111)-7×7 surface. Strain relaxation takes place in the incommensurate phase and results in the formation of periodic vacancies and C_{60} heptamer arrays. The strain relief patterns and coexistence of compressive and tensile strains in the incommensurate phase as well as the stripe domain walls constituted by antiphase boundaries in the commensurate phase have never been found in the previous C_{60} thin films, to the best of our knowledge.

II. EXPERIMENTS AND CALCULATIONS

The experiments were conducted in an ultra-high vacuum low temperature scanning tunneling microscopy (STM) (Unisoku USM1500) with a base pressure of 2.0×10^{-10} mbar. The Si(111)-7×7 substrate was prepared by overnight degassing at $\sim$800 K and subsequently flashing to 1500 K. Cd

_____

[*]Corresponding authors: skqtt@swu.edu.cn; jzwangcn@swu.edu.cn

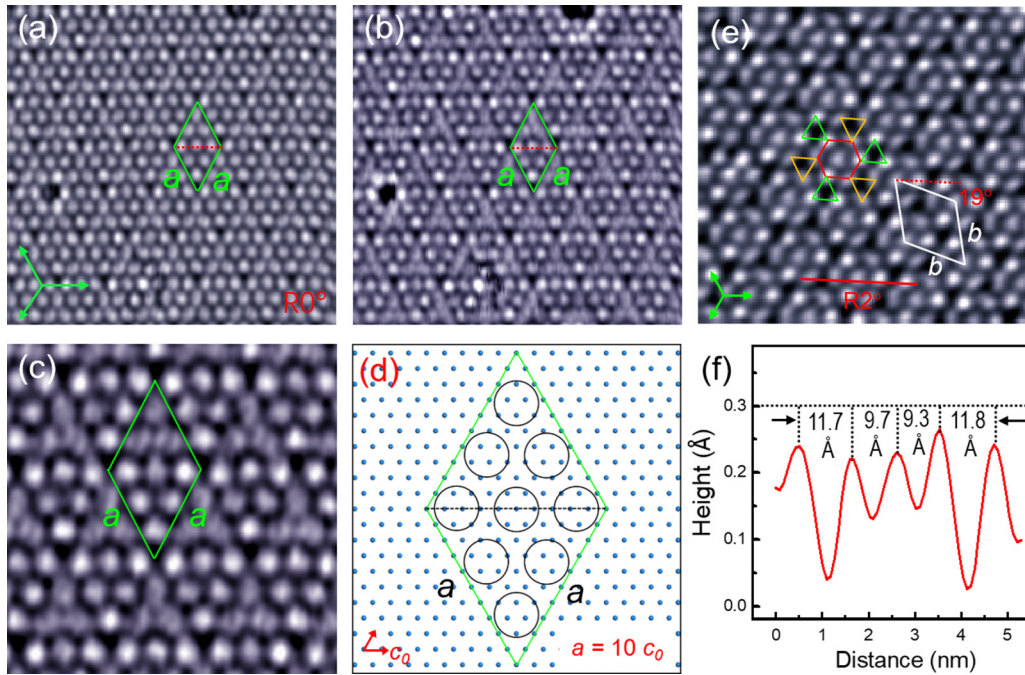FIG. 1. The 10×10 high-order commensurate (HOC) phase and incommensurate phase of C_{60} monolayer on Cd(0001). (a) Filled-state STM image of the HOC phase obtained by low-temperature deposition (200 K), -0.4 V. (b) Empty-state STM image of the HOC phase showing the distinct contrasts between the two half-unit cells (HUCs), 0.2 V. (c) Close-up view of the HOC phase, 0.2 V. (d) Schematic structural model of the 10×10 HOC phase. (e) Periodic vacancies and C_{60} heptamer arrays appeared in the incommensurate phase of R2° domain after annealing to RT, 1.5 V. (f) Line scan corresponding to the red line in (e). The images sizes are 20 nm$\times$19.5 nm for (a) and (b), 10 nm$\times$10 nm for (c), and 14.6 nm$\times$13.9 nm for (e).

atoms with a purity of 99.998% were thermally evaporated from a quartz crucible onto the Si(111)-7×7 surface. Flat and smooth Cd(0001) thin films were obtained by depositing $10 \sim 15$ monolayer (ML) of Cd. Due to the strong anisotropic electron motion with large lateral effective mass, the as-grown Cd(0001) thin films reveal a perfect electronic transparency such that the interfacial Si atoms can be clearly resolved. C_{60} molecules were evaporated from a home-made tantalum boat onto the Cd(0001) films. The substrate was kept at different temperature between 200 and 330 K so as to obtain different structures of C_{60} monolayer. Post-growth annealing the as-grown C_{60} films to room temperature (RT) was performed. STM images were acquired in constant-current mode at 77.6 K with the bias voltages applied at the samples.

The theoretical calculations were performed by using the ab initio simulation [33,34]. The electron-ion interactions were described with the projector augmented wave potentials [35,36] and the electronic exchange-correlation energy was treated by generalized-gradient approximation of Perdew-Burke-Ernzerhof [37]. The optB86b-vdW was employed to consider the nonlocal dispersion forces [38]. The adsorption calculations were conducted by playing various potential configurations of the C60 molecule on a Cd(0001) surface. The Cd(0001) surfaces were modeled by using a slab geometry with four atomic layers of a 5×5 unit cell and a ~20-Å vacuum layer. The kinetic energy cutoff for the plane-wave expansion was set to 400 eV. The k-point sampling in the Brillouin zone was implemented by the Monkhorst-Pack scheme with the grids of $3\times3\times1$. All of the atoms except for the bottom two Cd layers were fully relaxed within the residual force

smaller than 0.02 eV/Å. The simulated STM images were obtained using the constant current mode based on calculated charge densities.

III. RESULTS AND DISCUSSIONS

We start the experiment by depositing C_{60} molecules on Cd(0001) at low-temperature (~200 K). Figure 1(a) shows an "in phase" domain of the as-grown C_{60} monolayer. Each unit-cell contains nine C_{60} molecules: three in the upper HUCs, three in the lower HUCs, and the remaining three located at the border line between upper and lower HUCs. The arrangement of C_{60} molecules reveals a hexagonal lattice constant $a = 30 \pm 0.2$ Å, which is nearly ten times the lattice constant (2.97 Å) of Cd(0001) [39] It is slightly larger than three times of the preferred spacing (10.02 Å) in C_{60} crystals [40], corresponding to a very small (1.2%) compressive strain. Thus this in phase domain can be described as a 10×10 HOC phase or a 3×3 superstructure as displayed in Fig. 1(d).

In the empty-state STM image [Fig. 1(b)], the HOC phase exhibits two distinct contrasts between the upper and lower HUCs, similar to the well-known Si(111)-7×7 surface and the 7×7 superstructure of C_{60} on Au(111) [41]. As shown in the close-up view in Fig. 1(c), the three C_{60} molecules in the upper HUCs reveal a two-lobe contrast; while the other six C_{60} molecules exhibit a bright round protrusion without sub-molecular resolution. Based on the optimized configurations and simulated STM images of C_{60} on Cd(0001) [Figs. 2(a), 2(a′)], the two-lobe motif corresponds to the molecular orientation with 6:6 bond facing up, similar to the previous
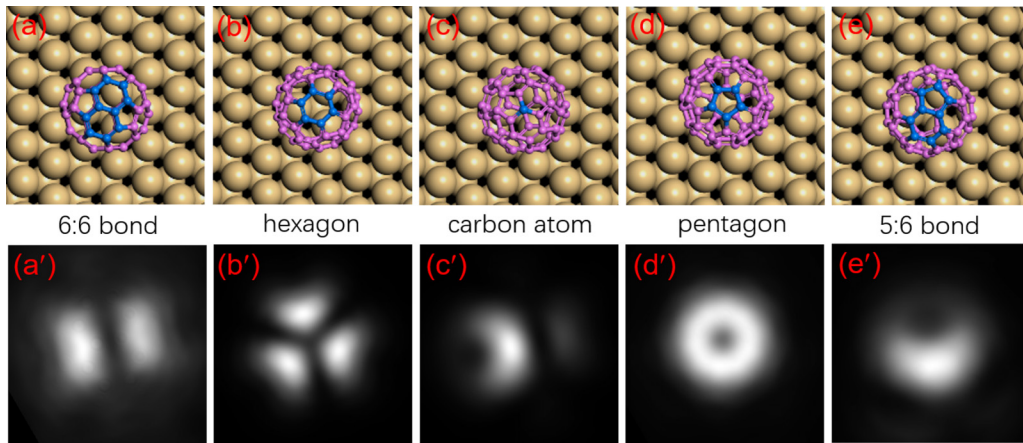
FIG. 2. Optimized configurations of a C_{60} molecule adsorbed on Cd(0001) surface. Top views of the structural models (a)–(e) and simulated empty-state STM images (a′)–(e′) of five kinds of high-symmetry orientations corresponding to the C_{60} with a 6:6 bond (a), (a′), hexagon (b), (b′), carbon atom (c), (c′), pentagon (d), (d′), and 5:6 bond (e), (e′) facing up, respectively.

observations of a C_{60} molecule on Au(111) and Cu(100) [12,41,45]. Most importantly, there are four corner holes appearing at the four apex positions of rhombus unit cells, which also appeared in the Si(111)-7×7 surface.

Interestingly, we found a structural transition from the HOC phase to an incommensurate phase induced by postannealing the sample to RT. As shown in Fig. 1(e), rotation epitaxy takes place in C_{60} monolayer through a small lattice rotation for 2° relative to the substrate lattice directions. We notice that periodic vacancies appeared in this domain such that the C_{60} molecules are no longer uniformly distributed on the substrate; instead, they are reorganized into the highly ordered arrays of individual C_{60} heptamer. As indicated by the white rhombus, the heptamers reveal a hexagonal lattice $b = 27.6 \pm 0.1$ Å and a misorientation angle of 19° with respect to the Cd(0001) lattices. The transformation matrix between the lattices of incommensurate C_{60} phase and Cd(0001) substrate can be described as [7, 3.5, −3.5, 10.4]. Each C_{60} heptamer is surrounded by six trigonal vacancies (three pointing down and three pointing up). Within the heptamer clusters, the central C_{60} molecule is surrounded by three bright and three dim molecules.

The formation mechanism of periodic vacancies around C_{60} heptamers can be attributed to the strain relaxation induced by rotation epitaxy. As revealed by Fig. 1(f), the height profile line demonstrates that the intermolecular spacing is not uniform. The C_{60}-C_{60} distance is 11.7 ∼ 11.8 Å between the heptamer clusters, but is reduced to 9.3 ∼ 9.7 Å; within the heptamers. It means that the C_{60} molecules are highly compressed inside the heptamers with compressive strain of 7.2%, but are strongly stretched outside the heptamers (within vacancies) with a tensile strain of 17.8%. In other words, compressive and tensile strains coexisted in this incommensurate phase, similar to the case of discommensurate reconstruction of Si(111)-Cu, Ga, and In systems [42]. According to the reported C_{60}-C_{60} spacing for C_{60} monolayers on Cu(111) [19] and Ag(111) [43], the 9.3-Å distance observed here represents the lower extreme value for C_{60} monolayer.

If we deposit C_{60} molecules directly at RT, instead of low-temperature deposition with postannealing, a com-

pletely different C_{60} monolayer can be obtained. As shown in Fig. 3(a), the C_{60} molecules form the commensurate $2\sqrt{3} \times 2\sqrt{3}$ R30° structure with parallel stripe domain walls. Based on the C-I phase transition theory, the stripe patterns of domain walls result from the repulsive interaction between the walls, due to the positive wall crossing energy [44]. Within the C_{60} domains, there are either three or four parallel molecular rows. The intermolecular spacing is 10.4 Å, slightly larger than the preferred spacing (10.02 Å) in the *fcc* C_{60} crystals. It means this incommensurate phase suffers a small tensile strain of 3.7%. As shown in the high-resolution images of Fig. 3(b), all C_{60} molecules reveal a bright round protrusion with a small off-center hole, similar to the C_{60} motif on Cu(100), Si(100)-2×1, and graphene [45–47]. Compared with the simulated image in Figs. 2(e), 2(e′), this motif corresponds to the molecular orientation with a 5:6 bond facing up. We also noticed that the C_{60} molecules from two neighboring domains adopt the opposite orientations, as indicated by the arrows at the two sided of domain walls. For this reason, the stripe domain walls may be also referred to as antiphase boundaries. We speculate that the opposite orientations of C_{60} molecules are helpful to release the tensile stress in the commensurate $2\sqrt{3} \times 2\sqrt{3}$ R30° domains. It should be pointed out that such a kind of parallel stripe domain walls (antiphase boundaries) has never been observed in the $2\sqrt{3} \times 2\sqrt{3}$ R30° phases reported previously, to the best of our knowledge. At first glance, these stripe domain walls resemble the linear-wall mazes in the metastable C_{60} phase on Cu(111). However, the former is a commensurate phase with $2\sqrt{3} \times 2\sqrt{3}$ reconstruction, while the latter is a high-order commensurate phase with a $p(2 \times 2)$ coincidence, where nearly 50% C_{60} molecules reveal a dim contrast.

In order to explore the electronic states of C_{60} molecules on Cd(0001), we performed scanning tunneling spectra measurements inside the commensurate $2\sqrt{3} \times 2\sqrt{3}$ domain. Figure 3(c) shows a representative conductance dI/dV spectrum acquired on top the individual C_{60} molecules. The peaks at −2.2 eV, 0.3–0.7 eV, and 1.9 eV correspond to the highest occupied molecular orbital (HOMO), the lowest unoccupied molecular orbital (LUMO), and the LUMO+1 states

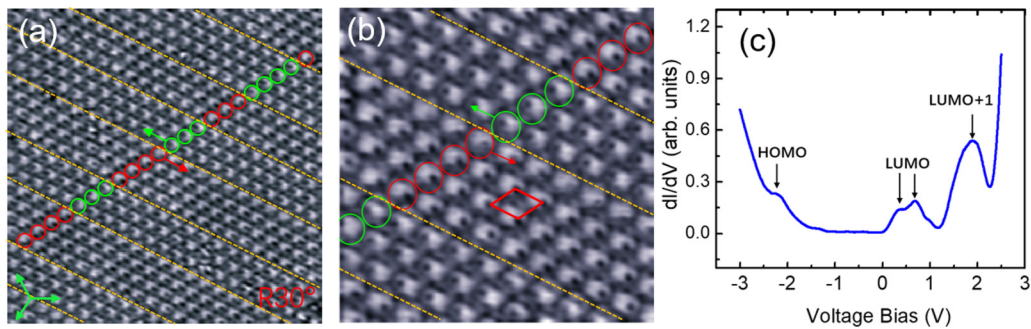FIG. 3. Stripe domain walls in the commensurate $2\sqrt{3}\times2\sqrt{3}$ R30° phase obtained by RT deposition. (a) The C_{60} molecules inside the two neighboring domains show the opposite orientations. The antiphase domain boundaries constitute stripe domain walls, 20 nm×20 nm, 1.8 V (b) Close-up view of the $2\sqrt{3}\times2\sqrt{3}$ R30° phase, 10 nm×10 nm, 1.8 V. The C_{60} molecules exhibit a bright round protrusion with a small off-center hole. (c) Differential conductance dI/dV spectrum acquired in the commensurate $2\sqrt{3}\times2\sqrt{3}$ R30° domain with a set point of $U = 1.0$ V, $I = 70$ pA. The LUMO level splits into two discrete peaks at 0.34 and 0.68 eV, respectively, and the HOMO-LUMO gap is 2.5 eV.

of C_{60} molecule, respectively. The gap between HOMO and LUMO is 2.5 eV, smaller than the situation of Au(111) and graphene/Cu(111) substrates [10,21]. The triply degenerate LUMO level splits into two discrete peaks at 0.34 and 0.68 eV. Such splitting can be attributed to the Jahn-Teller distortions of C_{60} molecules brought by the charge transfer from substrate to C_{60} molecules [47].

Figure 4(a) shows the topography of second layer of C_{60} grown at RT. The C_{60} molecules are arranged at the direction of 17° relative to Cd(0001) lattices. Interestingly, there is a kagome superstructure involving nineteen C_{60} molecules. The lattice constant of the kagome superstructure is 36.4 ± 0.2 Å, which is $\sqrt{13}$ times of C_{60}-C_{60} spacing ($c = 10.1 \pm 0.1$ Å). As shown in the close-up view [Fig. 4(b)], the C_{60} molecule at the hexagon centers reveals a three-lobe clover pattern, corresponding to the C_{60} orientation with hexagon facing up
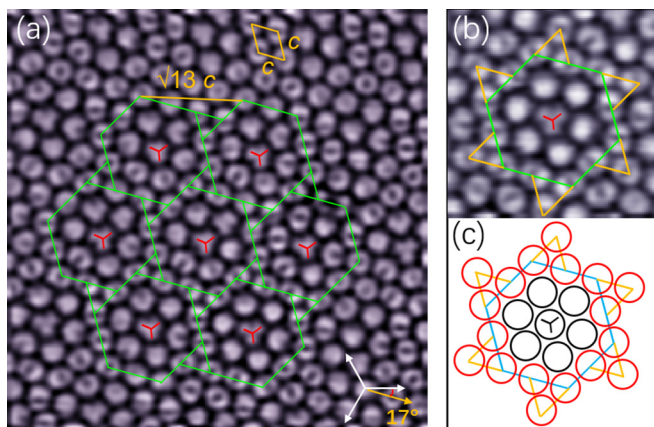
[Figs. 2(b), 2(b′)]. Around the central molecule, there are six C_{60} molecules located at the inner small hexagon (the first nearest-neighbor to the central molecule), and 12 molecules appeared at the outer large hexagon (the second nearest-neighbor to the central molecule). Most importantly, the 12 C_{60} molecules at the outer hexagon exhibit a two-lobe motif, corresponding to the C_{60} orientation with 6:6 bonding facing up [Figs. 2(a), 2(a′)]. Furthermore, the 12 molecules adopt different orientations like the petals in a flower. Previously, similar flower patterns were observed in the second C_{60} layer on Au(111), where a complex orientation order was identified [10]. As shown in the schematic model in Fig. 4(c), the kagome superstructure reveals a chiral feature: the six small triangles made of three molecules appear at the asymmetrical positions with respect to the outer large hexagon, constituting the anticlockwise pinwheel pattern. If we consider the inner small hexagon as a small "domain", then the 12 molecules located at outer large hexagon can be regarded as intersecting "domain walls". What is unique about such kinds of domain walls is that they release strains through adjusting the C_{60} orientations, rather than through changing the intermolecular distances as before.

Shown in Fig. 5(a) is a C_{60} monolayer island grown at elevated substrate temperature ($\sim$330 K). It is found that two types of triangular domains appear in this island. Within
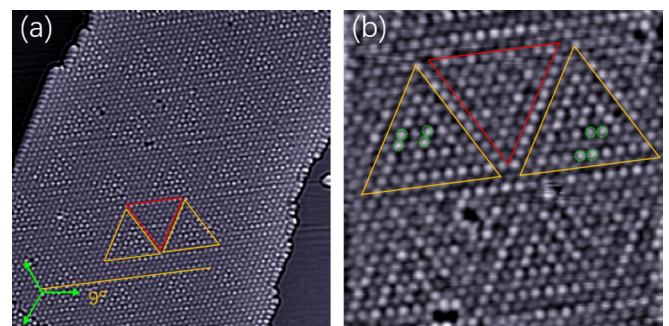

FIG. 4. Second C_{60} layer obtained by RT deposition. (a) Kagome structure showing $\sqrt{13}\times\sqrt{13}$ superstructure in a R17° domain, 15 nm×15 nm, −0.5 V. (b) Zoom-in image of the kagome structure, 6 nm×6 nm, −0.5 V. The central C_{60} molecule is surrounded by six molecules at the inner small hexagon and 12 molecules at outer large hexagon. (c) Schematic model of the kagome structure. The six small triangles made of three molecules are located at the asymmetric positions with respect to the large hexagon, constituting the anticlockwise pinwheel pattern.

FIG. 5. (a) A C_{60} monolayer island showing triangular domains formed at 330 K, 60 nm×60 nm, 0.4 V. (b) Close-up view of the triangular domain, 25 nm×25 nm, 0.4 V.

the domain marked by an up-triangle, the C_{60} molecules reveal a bright or dim contrast with an apparent height difference of 0.2 Å. At a first glance, the arrangement of bright molecules looks disordered, but close inspection indicates that they have a local 2×1 superstructure [Fig. 5(b)]. In the domains marked by a down-triangle, there are only very few bright molecules, most molecules show a dim contrast. Thus we refer to the two types of domains as bright and dim ones. Previous studies indicated that the dim C_{60} molecules reside in the vacancy or nanopit positions, while the bright molecules are located on top of substrate atoms. Thus we attribute the formation of triangular domains to the substrate reconstruction and vacancy formation at elevated temperature.

Both the bright and dim domains reveal a similar size of ∼10 nm. Due to the quasiperiodic arrangements of bright molecules, the domain boundaries between bright and dim domains are not very clear. Inside the bright and dim domains, the C_{60} molecules are aligned at the direction deviating for 9° from Cd(0001) lattices with a C_{60}-C_{60} distance of 10.56 Å, slightly larger than the bulk value (10.02 Å) in C_{60} crystals. Thus there is a small tensile strain of 5.3% inside the two types of domains.

IV. CONCLUSION

The C-I phase transition, rotation epitaxy, and strain relaxation patterns in C_{60} overlayer grown on Cd(0001) surface have been observed. When deposited at low temperature (∼200 K), the C_{60} molecules form a HOC phase with 10×10 reconstruction (3×3 superstructure), resembling the well-known Si(111)-7$\times$7 surface due to the presence of corner holes and two different HUCs. Postannealing the as grown C_{60} monolayer to RT leads to the structural transition from the HOC phase to an incommensurate structure. Strain relaxation occurs in the incommensurate domain such that periodic vacancies and C_{60} heptamer arrays form in this phase. When deposited on Cd(0001) at RT, C_{60} molecules form the commensurate $2\sqrt{3}\times2\sqrt{3}$ R30° phase, which contains parallel stripe domain walls. These results are helpful for gaining insight on the strain relaxation mechanism and for improving the quality of C_{60} thin films.

[1] H. Freimuth, H. Wiechert, H. P. Schildberg, and H. J. Lauter, Phys. Rev. B **42**, 587 (1990).

[2] J. C. Hamilton, R. Stumpf, K. Bromann, M. Giovannini, K. Kern, and H. Brune, Phys. Rev. Lett. **82**, 4488 (1999).

[3] K. R. Elder, C. V. Achim, E. Granato, S. C. Ying, and T. Ala-Nissila, Eur. Phys. Lett. **116**, 56002 (2016).

[4] C. R. Woods, L. Britnell, A. Eckmann, R. S. Ma, J. C. Lu, H. M. Guo, X. Lin, G. L. Yu, Y. Cao, R. V. Gorbachev, A. V. Kretinin, J. Park, L. A. Ponomarenko, M. I. Katsnelson, Y. N. Gornostyrev, K. Watanabe, T. Taniguchi, C. Casiraghi, H. J. Gao, A. K. Geim, and K. S. Novoselov, Nat. Phys. **10**, 451 (2014).

[5] L. L. Jiang, Z. W. Shi, B. Zeng, S. Wang, J. H. Kang, T. Joshi, C. H. Jin, L. Ju, J. H. Kim, T. Lyu, Y. R. Shen, M. Crommie, H. J. Gao, and F. Wang, Nat. Mater. **15**, 840 (2016).

[6] I. V. Lebedeva and A. M. Popov, Phys. Rev. B **99**, 195448 (2019).

[7] A. D. Novaco and J. P. McTague, Phys. Rev. Lett. **38**, 1286 (1977).

[8] J. P. McTague and A. D. Novaco, Phys. Rev. B **19**, 5299 (1979).

[9] J. A. Gardener, G. A. D. Briggs, and M. R. Castell, Phys. Rev. B **80**, 235434 (2009).

[10] L. Tang and Q. M. Guo, Phys. Chem. Chem. Phys. **14**, 3323 (2012).

[11] L. Tang, X. Zhang, Q. M. Guo, Y. N. Wu, L. L. Wang, and H. P. Cheng, Phys. Rev. B **82**, 125414 (2010).

[12] H. Shin, A. Schwarze, R. D. Diehl, K. Pussi, A. Colombier, E. Gaudry, J. Ledieu, G. M. McGuirk, L. N. Serkovic Loli, V. Fournee, L. L. Wang, G. Schull, and R. Berndt, Phys. Rev. B **89**, 245428 (2014).

[13] H. I. Li, G. J. P. Abreu, A. K. Shukla, V. Fournee, J. Ledieu, L. N. Serkovic Loli, S. E. Rauterkus, M. V. Snyder, S. Y. Su, K. E. Marino, and R. D. Diehl, Phys. Rev. B **89**, 085428 (2014).

[14] W. W. Pai and C. L. Hsu, Phys. Rev. B **68**, 121403(R) (2003).

[15] W. W. Pai, C. L. Hsu, K. C. Lin, L. Y. Sin, and T. B. Tang, Appl. Surf. Sci. **241**, 194 (2005).

[16] K. Pussi, H. I. Li, H. Shin, L. N. Serkovic Loli, A. K. Shukla, J. Ledieu, V. Fournee, L. L. Wang, S. Y. Su, K. E. Marino, M. V. Snyder, and R. D. Diehl, Phys. Rev. B **86**, 205406 (2012).

[17] T. Hashizume, K. Motai, X. D. Wang, H. Shinohara, Y. Saito, Y. Maruyama, K. Ohno, Y. Kawazoe, Y. Nishina, H. W. Pickering, Y. Kuk, and T. Sakurai, Phys. Rev. Lett. **71**, 2959 (1993).

[18] S. S. Wong, W. W. Pai, C. H. Chen, and M. T. Lin, Phys. Rev. B **82**, 125442 (2010).

[19] W. W. Pai, C. L. Hsu, M. C. Lin, K. C. Lin, and T. B. Tang, Phys. Rev. B **69**, 125405 (2004).

[20] H. Shin, S. E. ODonnell, P. Reinke, N. Ferralis, A. K. Schmid, H. I. Li, A. D. Novaco, L. W. Bruch, and R. D. Diehl, Phys. Rev. B **82**, 235427 (2010).

[21] M. Jung, D. Shin, S. D. Sohn, S. Y. Kwon, N. Park, and H. J. Shin, Nanoscale. **6**, 11835 (2014).

[22] L. Guo, Y. Wang, D. Kaya, Z. Wang, M. Zhang, and Q. M. Guo, Appl. Surf. Sci. **538**, 148142 (2021).

[23] L. Guo, Y. Wang, D. Kaya, R. E. Palmer, G. D. Chen, and Q. M. Guo, Nano Lett. **18**, 5257 (2018).

[24] D. V. Gruznev, A. V. Matetskiy, L. V. Bondarenko, O. A. Utas, A. V. Zotov, A. A. Saranin, J. P. Chou, C. M. Wei, M. Y. Lai, and Y. L. Wang, Nat. Commun. **4**, 1679 (2013).

[25] I. H. Hong, C. J. Gao, K. B. Lin, and C. C. Kaun, Appl. Surf. Sci. **531**, 147338 (2020).

[26] D. A. Olyanich, V. V. Mararov, T. V. Utas, L. V. Bondarenko, A. Y. Tupchaya, A. V. Matetskiy, N. V. Denisov, A. N. Mihalyuk, S. V. Eremeevc, D. V. Gruzneva, A. V. Zotov, and A. A. Saranin, Appl. Surf. Sci. **501**, 144253 (2020).

[27] D. A. Olyanich, V. V. Mararov, T. V. Utas, A. Y. Aladyshkin, A. N. Mihalyuk, A. V. Zotov, and A. A. Saranin, Appl. Surf. Sci. **456**, 801 (2018).

[28] D. V. Klyachko, J. M. Lopez-Castillo, J. P. Jay-Gerin, and D. M. Chen, Phys. Rev. B **60**, 9026 (1999).

[29] H. I. Li, K. J. Franke, J. I. Pascual, L. W. Bruch, and R. D. Diehl, Phys. Rev. B **80**, 085415 (2009).

[30] R. W. Stark and L. M. Falicov, Phys. Rev. Lett. **19**, 795 (1967).

[31] S. Daniuk, T. Jarlborg, G. Kontrym-Sznajd, J. Majsnerowski, and H. Stachowiak, J. Phys.: Condens. Matter **1**, 8397 (1989).

[32] H. S. Chauhan, L. Ilver, P. O. Nilsson, J. Kanski, and K. Karlsson, Phys. Rev. B **48**, 4729 (1993).

[33] G. Kresse and J. Furthmüller, Phys. Rev. B **54**, 11169 (1996).

[34] G. Kresse and J. Furthmüller, Comput. Mater. Sci. **6**, 15 (1996).

[35] P. E. Blöchl, Phys. Rev. B **50**, 17953 (1994).

[36] G. Kresse and D. Joubert, Phys. Rev. B **59**, 1758 (1999).

[37] J. P. Perdew, K. Burke, and M. Ernzerhof, Phys. Rev. Lett. **77**, 3865 (1996).

[38] J. Klimes, D. R. Bowler, and A. Michaelides, Phys. Rev. B **83**, 195131 (2011).

[39] D. A. Edwards, W. E. Wallace, and R. S. Crai, J. Am. Chem. Soc. **74**, 5256 (1952).

[40] P. A. Heiney, J. E. Fischer, A. R. McGhie, W. J. Romanow, A. M. Denenstein, J. P. McCauley, A. B. Smith III, and D. E. Cox, Phys. Rev. Lett. **66**, 2911 (1991).

[41] G. Schull and R. Berndt, Phys. Rev. Lett. **99**, 226105 (2007).

[42] J. Zegenhagen, P. F. Lyman, M. Bohringer, and M. J. Bedzyk, Phys. Status Solidi **204**, 587 (1997).

[43] K. A. Mansour, P. Ruffieux, W. Xiao, P. Gröning, R. Fasel, and O. Gröning, Phys. Rev. B **74**, 195418 (2006).

[44] P. Zeppenfeld, K. Kern, R. David, and G. Comsa, Phys. Rev. B **38**, 3918 (1988).

[45] J. Kröger, N. Néel, and L. Limot, J. Phys.: Condens. Matter **20**, 223001 (2008).

[46] H. Q. Wang, C. G. Zeng, B. Wang, J. G. Hou, Q. X. Li, and J. L. Yang, Phys. Rev. B **63**, 085417 (2001).

[47] S. Han, M. X. Guan, C. L. Song, Y. L. Wang, M. Q. Ren, S. Meng, X. C. Ma, and Q. K. Xue, Phys. Rev. B **101**, 085413 (2020).